X-RAY INTERFERENCE METHODS OF ELECTRON BEAM DIAGNOSTICS

O.Chubar, A.Snigirev, S.Kuznetsov, T.Weitkamp, ESRF, Grenoble, France
V.Kohn, Russian Research Center "Kurchatov Institute", Moscow

Abstract

Electron beam diagnostics methods based on interference and diffraction of synchrotron radiation (SR) in hard X-ray range will be discussed. Two simple optical schemes providing X-ray interference patterns highly sensitive to transverse size of the emitting electron beam, will be considered. For each scheme, the visibility of fringes in the pattern depends on transverse size of the electron beam. However, the pattern is also determined by the scheme geometry, shape and material of diffracting bodies. Therefore, for correct interpretation of the experimental results, high-accuracy computation of SR emission and propagation in the framework of physical optics should be used. Examples of practical measurements and processing of the results are presented.

1 INTRODUCTION

Visible light interference methods have proved to be very efficient for diagnostics of relativistic charged particle beams emitting synchrotron radiation in magnetic fields of accelerators [1-6]. Nevertheless, since 3rd-generation SR sources are mainly dedicated for X-rays, the use of X-rays for electron beam diagnostics in these accelerators can be advantageous. Such diagnostics can be based on the same equipment that is used in other experiments; besides, it may offer higher resolution.

A number of X-ray experimental techniques benefiting from high spatial coherence of the SR, e.g. phase-contrast imaging, holography, interferometry, have been developed [7-11]. These techniques require characterisation and "in-place" control of the source coherence, which makes the X-rays based beam diagnostics further important.

This paper considers two very simple diffraction/ interference schemes, which can be readily used for beam diagnostics at any X-ray beamline (not necessarily fully dedicated for the diagnostics). One is the well-known Fresnel diffraction at a slit, and the other is a wavefront-splitting interference scheme where a thin fiber is used as an obstacle and phase-shifting object. As different from previous considerations made for isotropic source with finite transverse size [12-14], the current paper takes into account peculiarities of synchrotron (undulator) radiation emitted by an electron beam with finite transverse emittance (i.e., not only with the size, but also with angular divergence).

2 BASICS OF THE METHODS

2.1 Isotropic Source with Finite Transverse Size

Let us recall that in the case when a source has finite transverse size, and different points of the source emit incoherently, the resulting intensity of the radiation passed through an optical system to a detector plane is obtained by summing up intensities of emission from all points of the source [15]:

$$I(x,y) = \iint I_0(x,y;x_s,y_s)\, B(x_s,y_s)\, dx_s dy_s \,, \qquad (1)$$

where (x,y) are transverse coordinates in the detector plane, (x_s,y_s) transverse coordinates at the source, I_0 intensity from a point source (referenced below as point-source intensity), and B the source brightness.

For many simple diffraction and interference schemes with a source emitting spherical waves, in small-angle approximation, Eq. (1) is a convolution-type integral, i.e.:

$$I_0(x,y;x_s,y_s) \approx \tilde{I}_0(x - m x_s, y - m y_s)\,, \qquad (2)$$

where $m = -r_d / r_s$ is a "magnification" factor, with r_s being distance from the source to an obstacle, and r_d distance from the obstacle to the detector (see Fig. 1). We note that this effect is used in pinhole cameras (which are successfully applied for electron beam diagnostics [16]).

If Eq. (2) is valid, $\tilde{I}_0(x,y)$ is known, and the resulting intensity $I(x,y)$ is measured to a sufficient accuracy, one can try to reconstruct $B(x_s,y_s)$ using the Wiener filtering [17] or a regularization technique [18].

The resolution of an optical scheme at the source size measurement depends on the point-source intensity $\tilde{I}_0(x,y)$. In the case of Fresnel diffraction at a slit, $\tilde{I}_0$ possesses fringes with the widths on the order of $\lambda r_d/a$, where λ is the radiation wavelength and a the slit size. This can be compared with the source image size $\sigma r_d/r_s$. However, the resolution of this scheme can be much better, because $\tilde{I}_0$ has also smaller details originating from "interaction" of the slit edges (see Fig. 2).

Figure 1: Interference pattern formation from a source with finite transverse size.

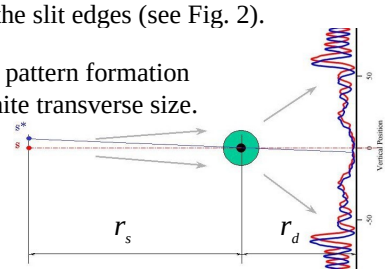

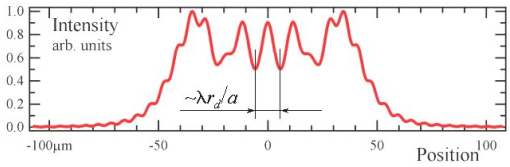

Figure 2: Point-source intensity distribution at the Fresnel diffraction at a slit.

2.2 *Finite-Emittance Electron Beam*

This section describes how a more accurate computation of the SR emitted by an electron beam and propagated through an optical system, can be performed. Such a computation allows to verify whether a particular approximation corresponds to realistic experimental conditions, and thus to choose an adequate simplified model and method for processing the experimental results.

Starting from Fourier transformations of the retarded potentials, one can obtain the following expression for the frequency-domain electric field of radiation emitted by a relativistic electron (Gaussian System) [19]:

$$\vec{E} = iek \int_{-\infty}^{+\infty} [\vec{\beta} - \vec{n}[1 + i(kR)^{-1}]] R^{-1} \exp[ik(c\tau + R)] d\tau, \quad (3)$$

where k is a wave number, $\vec{\beta} = \vec{\beta}(\tau)$ instant relative velocity of electron, $\vec{n} = \vec{n}(\tau)$ unit vector directed from instant electron position to an observation point, $R = R(\tau)$ distance from the electron to the observation point, c speed of light, e charge of electron. Eq.(3) describes practically all kinds of single-electron emission in the near- and far-field observation regions. It allows to compute SR electric field at some longitudinal position, e.g. before the first optical element of a beamline. Typically, only transverse components of the electric field (3) need to be considered.

The wavefront propagation through transmission optical elements can be simulated by multiplication of the transverse electric field by a complex transmission function of transverse position, which can take into account both attenuation and phase shift of the wave field.

Assuming small angles and distances considerably larger than wavelength, the transverse component of the electric field propagated through a drift space $\vec{E}_{\perp 2}$ can be computed from the electric field $\vec{E}_{\perp 1}$ before the drift space by the well-known Huygens-Fresnel principle

$$\vec{E}_{\perp 2} = -ik(2\pi)^{-1} \iint_{\Sigma} \vec{E}_{\perp 1} S^{-1} \exp(ikS) d\Sigma, \quad (4)$$

where S is a distance from a point on this surface to an observation point. If the integration surface Σ is (a part of) a plane perpendicular to the optical axis, and the observation points belong to another plane perpendicular to the optical axis, then Eq. (4) is a convolution-type integral that can be quickly computed by applying the convolution theorem and 2D FFT.

To obtain intensity distribution of the SR emitted by the finite-emittance electron beam, one needs to sum-up intensities obtained after propagation of electric fields from individual electrons. In general case, the single-electron intensity I_0 depends on transverse coordinates, angles and energy of the electron $(x_s, y_s, x_s', y_s', E_s)$, so that the final intensity is derived by integration with respect to all these variables:

$$I(x,y) = \int I_0(x,y;x_s,y_s,x_s',y_s',E_s) \times n(x_s,y_s,x_s',y_s',E_s)\, dx_s dy_s dx_s' dy_s' dE_s \quad (5)$$

where n is particle distribution in the beam phase space.

For different types of SR and different optical schemes, the single-electron intensity I_0 may not strongly depend on some of the phase-space variables. In each particular case, this dependence, as well as the validity of the convolution approximation (e.g. Eq.(2)), can be checked numerically, by making single-electron wavefront propagations for different values of $(x_s, y_s, x_s', y_s', E_s)$.

When performed for the Fresnel diffraction of undulator radiation (UR) at a slit, this test showed that if angular aperture of the slit is comparable to the opening angle of the single-electron UR, and to the electron beam angular divergence, then the latter can contribute to the final intensity distribution of the diffracted radiation. This contribution is typically smaller than that of the beam transverse size, however it should be taken into account at the process of results, of the beam diagnostics measurements.

The numerical methods based on Eqs.(3)-(5) are implemented in the SRW, a physical optics computer code for synchrotron radiation [20].

3 MEASUREMENTS

The measurements of Fresnel diffraction and the interference from a fiber were carried out at ID22 beamline of ESRF, using the radiation from a planar undulator (38 periods of 42 mm) at 11 keV photon energy. After the undulator, the radiation was deflected horizontally by a mirror (in order to suppress high-energy part of the UR spectrum), and then passed through a double-crystal monochromator.

In the Fresnel diffraction scheme, a 100 μm x100 μm rectangular slit was located at 37.6 m distance from the middle of the undulator, and the distance from the slit to detector was 5.5 m.

In another scheme, a cylindrical boron fiber was placed at a distance of 40.6 m from the undulator, and the detector was located at 1.85 m after the fiber. The diameter of the fiber was 100 μm; the fiber possessed a tungsten core with a diameter of ~15 μm.

The intensity distributions in the two schemes were registered by a 2D coordinate-sensitive detector consisted of a 1 μm thick YAG scintillator coupled by a visible light microscope to a CCD camera. The re-focused CCD pixel size was 0.24 μm, and the resolution, estimated as FWHM size of the point-spread function, was on the order of1 μm. The intensity distributions registered in the two schemes are shown in Fig. 3 on the left.

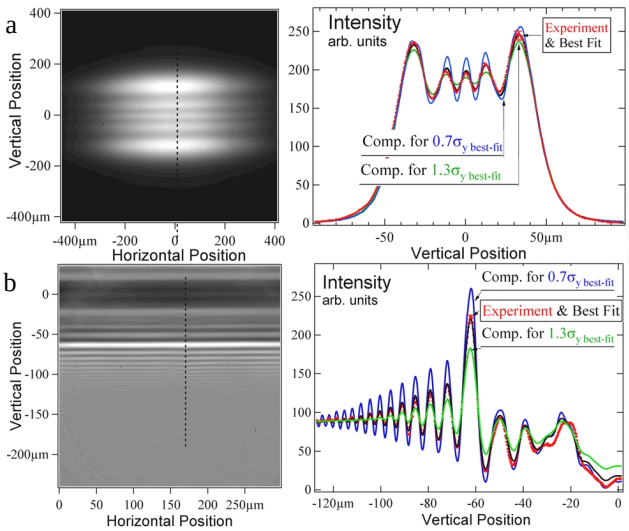

Figure 3: Measured intensity distributions and results of the fitting procedure for the Fresnel diffraction at a slit (a) and interference from a boron fiber (b).

The right-hand plots in Fig. 3 illustrate the fitting of vertical slices of the measured intensity by distributions computed for different values of vertical electron beam emittance ε_y, using a numerical procedure based on Eqs. (3)-(5). At the fitting, the vertical beam size and divergence were re-calculated for the middle of the straight section via:

$$\sigma_y = (\varepsilon_y \beta_y)^{1/2}; \quad \sigma'_y = (\varepsilon_y / \beta_y)^{1/2}, \qquad (6)$$

with the value of the vertical beta function assumed to be known: β_y = 2.5 m [21]. The particle distribution in the electron beam was assumed Gaussian over vertical position and angle. The detector point-spread function was approximated by the Gaussian as well.

The vertical RMS beam size value obtained from the Fresnel diffraction measurements is: $\sigma_y = 22 \pm 4$ μm, and from the interference at the fiber: $\sigma_y = 24 \pm 5$ μm. These values are larger than the vertical beam size value in the middle of a straight section which follows from the ESRF pinhole camera measurements performed at larger β_y [21]. The most probable reason for this discrepancy is the presence of the mirror and the vertically reflecting crystal monochromator in the optical scheme. These two optical components were not taken into account at processing of the experimental results, however, each of them could reduce the transverse coherence of the wavefront, due to imperfections of the mirror surface and possible contribution of the crystal transfer function, respectively.

5 CONCLUSIONS

X-ray diffraction and interference schemes can be used for beam diagnostics in 3rd-generation SR sources. The schemes are very simple and can be applied nearly at any X-ray beamline. This diagnostic has a very high theoretical resolution: on the order of microns. However, it is also very sensitive to the quality of optics. Therefore, to avoid systematic errors, transfer functions of the optical elements should be known to a reasonable accuracy; the use of transmission X-ray optics is preferable.

On the other hand, this type of measurements and data processing can be applied to characterize the transverse coherence properties of an entire X-ray beamline, including both the source and the optics in use.

REFERENCES

[1] T.Shintake et.al., "Experiments of nanometer spot size monitor at FFTB using laser interferometry", Proc. of IEEE PAC-95, p.2444
[2] O.Chubar, "Transverse electron beam size measurements using the Lloyd's mirror scheme of synchrotron light interference", Proc. of IEEE PAC-95, p.2447.
[3] Å.Andersson, M.Eriksson and O.Chubar, "Beam profile measurements with visible synchrotron light on MAX-II", Proc. of EPAC-96, p.1689.
[4] T.Mitsuhashi, "Spatial coherency of the synchrotron radiation at the visible light region and its application for the electron beam profile measurement", Proc. of IEEE PAC-97, p.766.
[5] S.Hiramatsu et. al., "Measurement of small beam size by the use of SR interferometer", Proc. of IEEE PAC-99, p.492.
[6] N.V.Smolyakov, "Interference diagnostics for storage ring electron beam", Nucl. Instr. and Meth., 1998, vol.A405, p.229.
[7] A.Snigirev, I.Snigireva, V.Kohn, S.Kuznetsov and I.Schelokov, "On the possibilities of X-ray phase contrast micro-imaging by coherent high-energy synchrotron radiation", Rev. Sci. Instrum., 1995, vol.66(12), p.5486.
[8] A.Snigirev, "Hard X-ray microscopy with coherent light: holography, phase contrast and interferometry", ICFA Workshop on 4th Generation Light Sources, Jan. 22-25 1996, ESRF, Grenoble.
[9] C.Raven, A.Snigirev, I.Snigireva, P.Spanne, A.Souvorov and V.Kohn, Appl. Phys. Lett., 1996, vol.69, p.1826.
[10] P.Cloetens, R.Barret, J.Baruchel, J.P.Guigay and M.Schlenker, J.Phys. D: Appl. Phys., 1996, vol.29, p.133.
[11] T.E.Gureyev, C.Raven, A.Snigirev, I.Snigireva and S.W.Wilkins, J.Phys. D: Appl. Phys., 1999, vol. 32, p.563.
[12] A.Snigirev, V.Kohn, I.Snigireva, "Fresnel diffraction by slits", in "ESRF Highlights 1996/1997", Nov.1997, p.91.
[13] V.Kohn, I.Snigireva and A.Snigirev, "Direct measurement of transverse coherence length of hard X-rays from interference fringes", Phys. Rev. Lett., 2000, vol.85(13), p.2745.
[14] V.Kohn, I.Snigireva, A.Snigirev, "Interferometric characterization of spatial coherence of high energy synchrotron X-rays", submitted to Elsevier Preprint.
[15] M.Born, E.Wolf, Principles of Optics, 4th ed., Pergamon Press, 1970.
[16] P.Elleaume et. al., "Measuring beam size using X-ray pinhole camera", J. Synchrotron Rad., 1995, vol.2, p.209.
[17] L.R.Rabiner, B.Gold, Theory and application of digital signal processing, EnglewoodCliffs, N.J.: Prentice-Hall, 1975.
[18] AN.Tikhonov, A.V.Goncharsky, V.V.Stepanov, "Inverse problems in image processing", in Ill-posed problems in natural sciences, Moscow: Mir Publishers, 1987.
[19] O.Chubar, "Precise Computation of Electron Beam Radiation in Non-uniform Magnetic Fields as a Tool for the Beam Diagnostics", Rev. Sci. Instrum., 1995, vol.66 (2), p.1872.
[20] Synchrotron Radiation Workshop (SRW) computer code is available from: http://www.esrf.fr/machine/support/ids/Public/Codes/software.html
[21] P.Elleaume, http://www.esrf.fr/machine/support/ids/Public/Sizes/sizes.html

This work was supported by INTAS Project No. 99-0469